Eco-Speed Advisory System for Electric Vehicles Incorporating Driver Preferences

Roberto Lot, James M. Fleming, Boli Chen, Simos A. Evangelou

***Abstract*—An eco-speed advisory system for front-wheel drive electric vehicle is proposed in this paper, demonstrating that including an optimal control model of driver preferences in such systems can successfully blend the objective of energy-efficiency with the subjective goals of human drivers, including desired following distances and time headways, a desired vehicle speed, smooth vehicle acceleration, and a comfortable corner negotiation speed. This builds on previous works that developed driver preference models for optimal control, but did not apply them to a realistic model of an EV powertrain to evaluate potential energy savings in practice. The resulting optimal control problem (OCP) is simplified for implementation by using a polynomial approximation of vehicle losses, and a relaxation of regenerative braking constraints that accurately accounts for required braking bias in a front-wheel drive vehicle. In testing, over a 25km journey involving rural, motorway and urban sections, blending driver preferences with energy efficiency in this framework achieves energy savings of 21% with only a 7% decrease in average speed. For car-following scenarios, 10–15% energy savings are achievable with no decrease in average speed.**

***Index Terms*—Optimal control, Electric vehicles, ADAS, Eco-driving, Driver modelling.**

I. Introduction

Environmental concerns and the drive towards greater energy efficiency poses great challenges for the automotive industry, making it more urgent to reduce the energy consumption of motor vehicles. There are two major research trends with the aim to reduce energy usage and cut emissions of road vehicles: a) electrification of vehicle powertrains [1], and b) guiding of drivers towards a more environmentally friendly driving style referred to as eco-driving [2].

Electrified vehicles, such as battery electric vehicles (EVs) and hybrid electric vehicles (HEVs), are currently intensively investigated and manufactured by the automotive industry, and receive profound focus in academic research [3]. Recently, the marketability of electrified vehicles has become a widely discussed issue. Range anxiety and a high cost make EVs and HEVs less favourable for private users. Therefore, there is an ongoing effort to push for even more energy efficient electrified powertrains and to make them more cost-effective. The energy efficiency of these vehicles can be improved by refining the motor design and choice of energy storage systems [4]. For HEVs, an essential measure is to improve the energy management systems, such that the powertrain is operated more efficiently [5]. In the past decade, the energy management problem of electrified powertrains has been investigated extensively with a range of proposed strategies, both rule-based and optimisation based (e.g. [6], [7]). However, the energy consumption calculation in such studies generally assumes the vehicle motion follows predefined drive cycles, so the influence of driver behaviour on the energy usage, for example when following other traffic, is not considered.

There is a significant body of work in eco-driving, in which it has been shown that the way a vehicle is driven can significantly affect the overall fuel use and subsequent emissions. Research has estimated that 5-10% of fuel can be saved if drivers pursue a more fuel efficient, economical and environmentally friendly driving style . In general, eco-driving behaviours can be studied in different scenarios such as: car following [8], cornering [9], intersection crossing with traffic lights [10] and varying road grade [11]. Ojeda, Luis Leon, et al. [12] and Han, Jihun, et al. [13] proposed speed advisory systems for connected vehicles which can generate a near-optimal speed profile. Numerically, the problem is solved using a Model Predictive Control-like approach in which real-time implementation is possible by the analytical solution of a state-constrained Optimal Control Problem (OCP). Kamal et al. [14] presented an eco-driving assistance system for a host vehicle that uses information including the state of the preceding vehicle, road gradients and the state of upcoming traffic signals. A multi-objective cost function is used for the optimal control problem formulation, which not only maximizes fuel economy but also regulates a safe headway distance. Model predictive control (MPC) is used to drive the vehicle optimally by anticipating upcoming road traffic.

Despite the contributory work, these existing eco-driving techniques neglect the preferences and comfort of the human driver in order to follow the optimised speed profile. In the present work, a driver preference model developed in [15], [16] is adopted which takes into account the naturalistic driver preferences in terms of speed, vehicle spacing, acceleration, and cornering speed. For a speed advisory system, the goal is to generate a reference speed profile based on available information about the ego vehicle and its environment, so that by following this reference profile the vehicle will meet performance criteria such as reducing energy consumption and ensuring the safety of the vehicle.

The specific contributions over the existing literature are:

- We develop an OCP for EV speed advisory which incorporates both realistic EV powertrain and vehicle losses and driver preferences on following distances, cornering speeds, and accelerations. This builds on the OCP framework previously developed in [15], [16], which considered driver preference models but not accurate energy losses for a front-wheel drive (FWD) EV powertrain.

Corresponding author: j.fleming@lboro.ac.uk. James Fleming is with the Wolfson School of Engineering, Loughborough University, UK. Boli Chen is with the Department of Electronic and Electrical Engineering, University College London, UK. Simos Evangelou is with the Department of Electrical and Electronic Engineering, Imperial College London, UK. Roberto Lot is with the Department of Industrial Engineering, University of Padova, Italy.

- For solution by direct methods, the eco-driving OCP is reformulated as one of minimising energy loss, with a polynomial fit for energy losses in the powertrain. To include limits resulting from braking bias for a FWD vehicle, a constraint is included on regenerative braking force, which is relaxed to an inequality to solve the OCP.
- We test the method in several scenarios, using a detailed model of an electric vehicle including drag, rolling resistance, mechanical braking losses, DC and AC converter efficiencies, and a realistic motor efficiency map. Cornering, car-following, and whole-journey scenarios are considered, based on a real-world driving route near Southampton, UK, with naturalistic driving data used for the lead vehicle in the car-following case.

The details of the work are given in the following sections, in particular Section II describes the modelling of the electric vehicle, then Section III gives the OCP incorporating the driver preference model. Section IV applies the developed methods to some simple test cases and a 25 km example driving scenario. Conclusions are given in the final section.

II. Electric Vehicle Modelling

A front-wheel driven electric vehicle (EV) is modelled taking into account the major vehicle and powertrain losses, with regenerative braking to improve the overall efficiency.

A. Longitudinal dynamics

According to Newton's second law, the longitudinal dynamics of the EV can be summarised as:

$$m\dot{v} = F - \frac{1}{2}\rho A C_d v^2 - mg\left(c_{rr}\cos\theta + \sin\theta\right) \tag{1}$$

where v is the vehicle speed, F is the overall wheel force, and θ the road gradient; the remaining parameters are specified in Table I. We find convenient to split the overall longitudinal force, which is positive under traction and negative under braking, into three *non-negative* components

$$F = F_p - F_r - F_f \tag{2}$$

where F_p is the propulsion force, and F_r and F_f are braking forces due to regenerative and hydraulic braking respectively.

B. Powertrain model

As shown in Figure 1, the powertrain contains a battery pack, which powers a synchronous electric motor via power converters (a DC-DC converter and a DC-AC inverter), with the motor then coupled to the front wheels via a reduction gear. The powertrain operation is reversible and allows regenerative braking, in which case the power flow is opposite in direction to the power flow when driving.

The motor shaft and the wheel axle are connected via a fixed gear transmission, which is modelled with a constant efficiency η_t. The motor speed ω_m can be calculated from the vehicle speed v as

$$\omega_m = \frac{N}{r}v \tag{3}$$

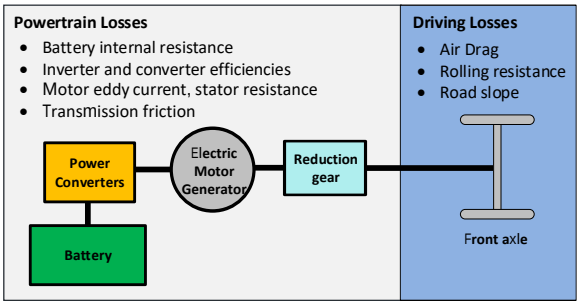

Fig. 1. Electric vehicle powertrain structure and losses considered.

where N is the gear ratio and r is the wheel radius. The motor torque T_m, which is positive for propulsion and negative under regenerative braking, is equal to

$$T_m = \frac{r}{N}\left(\frac{F_p}{\eta_t} - \eta_t F_r\right). \tag{4}$$

The main losses in the electrical system include electric motor/generator losses due to stator resistance, eddy currents, bearing friction, and aerodynamic resistance, and inverter and converter losses. For our present work, we adapted a permanent magnet motor from ADVISOR [17], for which the main characteristics are given in Table I and an efficiency map is illustrated in Figure 2. The latter is given as a function of the speed and torque

$$\eta_m = \eta_m(\omega_m, T_m) \tag{5}$$

For simplicity, the total efficiency of the power converters η_{pc} is assumed constant. The electric power that must be provided by the battery (output) to the power unit reads

$$P_b = \frac{F_p v}{\eta_t \eta_m \eta_{pc}} - \eta_t \eta_m \eta_{pc} F_r v \tag{6}$$

The open circuit voltage of the battery depends on the state of charge, where the largest variations occur either at low or high values of charge [18]. For the sake of simplicity, we neglect this variability and assume that the open circuit voltage E_0 is constant. We further assume that the battery internal resistance R_b is constant. Therefore, the balance among battery power output, voltage, and current i_b reads:

$$P_b = E_0 i_b - R_b i_b^2 \tag{7}$$

The battery current can therefore be calculated as

$$i_b = \frac{E_0 - \sqrt{E_0^2 - 4R_b P_b}}{2R_b} \tag{8}$$

where i_b is positive when discharging the battery, and negative under regenerative braking. In conclusion, the overall powertrain efficiency may be calculated as

$$\eta = \begin{cases} \frac{F_p v}{E_0 i_b} & \text{propulsion} \\ -\frac{E_0 i_b}{F_r v} & \text{braking} \end{cases} \tag{9}$$

and it is illustrated in Figure 2.

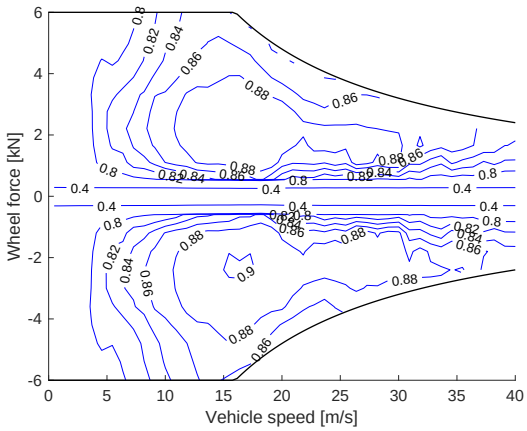

Fig. 2. Powertrain efficiency as a function of the vehicle speed and wheel force (force is positive under propulsion and negative under regenerative braking, efficiency accounts for the losses of the mechanical transmission, electric motor/generator, power converter, and battery).

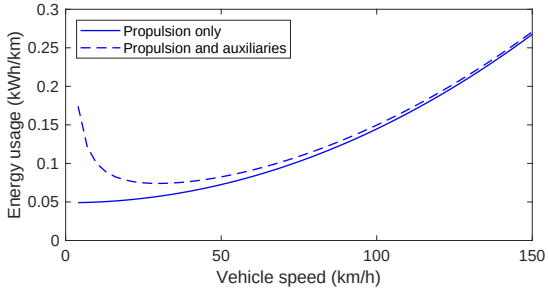

Fig. 3. Specific energy usage while driving at constant speed (the solid line neglects idle losses, the dotted line accounts for an idle power loss of 500 W).

Finally, the electrical energy consumption reads

$$E_b = \int_0^T (E_0 i_b + L_i)\ \mathrm{d}t \tag{10}$$

while T is the travel time and L_i are the idle power losses that are necessary to sustain vehicle auxiliary systems and are not included in Equation (6).

For our present work, we consider a compact hatchback BEV, with parameters as summarised in Table I. The specific energy usage at constant speed is illustrated in Figure 3 by considering a constant idle power $L_i = 500$ W (dotted line) and without idle power losses (solid line). Without idling losses, the specific energy usage increases monotonically with the speed, while the introduction of idle power significantly increases the specific energy usage at very low speed, so that a minimum is found at a speed of approximately 35 km/h.

C. Regenerative braking

Under braking, the electric power unit can be used as a generator and recover a significant amount of energy. To ensure braking performance and safety, the braking system is completed by front and rear hydraulic brakes. Braking management is not trivial and, in order to maximise the directional stability of the vehicle, the front versus rear braking

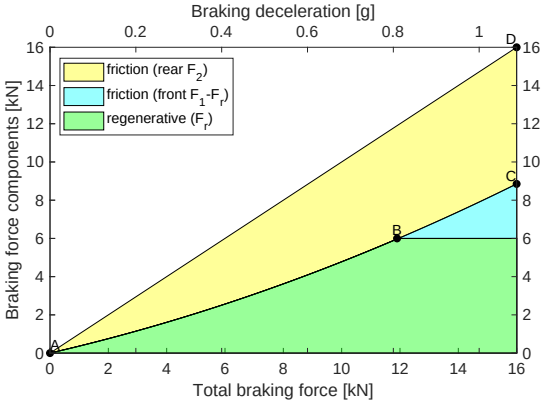

Fig. 4. Braking force distribution and regenerative braking. (the maximum regenerative torque, and the resulting position of B along curve AC, decreases for speeds greater than 16 m/s due to the power limits of the motor).

force distribution is not constant. More specifically, by considering moment equilibrium of the vehicle while decelerating, the braking forces F_1, F_2 that grant the same ratio between braking force on the contact patch and vertical reaction forces at the front and rear axle respectively read [19]

$$\begin{aligned} F_1 &= \frac{l_2 + h\,(F_r + F_f)}{l_1 + l_2}\,(F_r + F_f) \\ F_2 &= \frac{l_1 - h\,(F_r + F_f)}{l_1 + l_2}\,(F_r + F_f) \end{aligned} \tag{11}$$

where l_1, l_2 are the distances between the vehicle centre of mass and the front and rear axles respectively, while h is the centre of mass height. This force distribution is illustrated in Figure 4 as a function of the overall braking force, while a second axis on the top of the figure also indicates the braking deceleration achieved at low speed, i.e. when air drag is negligible. It is apparent that the front braking (area enclosed below the line ABC) increases more than, and the rear braking (area enclosed by points ABCD) increases less than proportionally to the overall braking force. Under severe braking, when the total braking force is larger than its value at point B, the requested front wheel force exceeds the generator operating range, which is limited both in torque and in power, therefore it is necessary to use friction brakes also. We note that the curve AB can be effectively approximated by a straight line (proportional relationship to the total braking force), therefore the regenerative braking force can be calculated as

$$F_r = \beta_r (F_r + F_f) \tag{12}$$

where β_r is a constant *regenerative braking bias*, until the torque or power limits of the electric motor are exceeded.

III. Eco-Driving Optimal Control Problem

A. Naturalistic driver preference model

In [16], the authors introduced a driver behaviour model that replicates car-following behaviour in a similar fashion to the well known Intelligent Driver Model (IDM) [20], but in addition is capable of replicating driver speed choice when

TABLE I
VEHICLE CHARACTERISTICS AND PHYSICAL PARAMETERS

Symbol	Value	Description
		Vehicle parameters
m	1500 kg	vehicle mass
l_1	1.65 m	centre of gravity distance from the front axle
l_2	1.75 m	centre of gravity distance from the rear axle
h	0.5 m	centre of gravity height
$\rho A C_d$	0.86 kgm^{-1}	coefficient of drag
c_{rr}	0.01	coefficient of rolling resistance
r	0.330 m	radius of the wheels
N	3.8	reduction gear ratio
$\eta_t \eta_{pc}$	0.97	combined transmission and electrical efficiency
$Q_{\max}$	40 kWh	battery capacity
E_0	400 V	battery open circuit voltage
R_b	0.0533 Ω	battery internal resistance
$P_{m,\max}$	80 kW	Motor peak power
$T_{m,\max}$	280 Nm	Motor maximum torque
$T_{r,\max}$	280 Nm	Generator maximum torque
$P_{r,\max}$	80 kW	Generator peak power
β_r	0.5	regenerative braking bias
		Driver model parameters
u_a	2.5 m/s^2	driver's acceleration preference
u_b	3.0 m/s^2	driver's braking preference
s_0	2.5 m	desired stationary headway distance
v_d	31.2 m/s	desired speed
τ	1.5 s	desired minimum time gap between vehicles
δ	4	IDM acceleration exponent
Γ	3 m/s^2	maximum admissible lateral acceleration
Δ	0.002rad^{-1}	driver's safety margin of curvature estimation

cornering and may be incorporated into OCPs. This model is phrased as the minimisation of a cost function:

$$J_d = \int_0^T L_d \ \mathrm{dt} \tag{13}$$

where the stage cost L_d is defined as

$$L_d = \delta^2 \left(\frac{v}{v_d} - 1\right)^2 + \gamma(v) \ \frac{(s/s_d - 1)^2}{(s/s_d)^2 + 1} + \left(\frac{u_a}{a}\right)^2 + \left(\frac{u_b}{b}\right)^2 \tag{14}$$

and where s, v, u_a, and u_b are the headway distance, ego vehicle speed, ego vehicle acceleration, and ego vehicle braking deceleration respectively, the parameter v_d is the desired vehicle speed, which is the speed the driver will take on a straight road without traffic, and s_d is a desired following distance given by

$$s_d = s_0 + \tau v \tag{15}$$

with s_0 and τ defined in Table I. Minimising the first term in (14) represents the urge to reduce travel time by driving close to this speed, where the parameter δ corresponds to the acceleration exponent in the IDM [20]. The second term is a headway distance penalty that becomes large for small s, has a minimum at s_d, then tends to a constant positive value as s becomes large to represent the driver's indifference to far away vehicles. The weighting function γ depends on the velocity and is given by:

$$\gamma(v) = 8 \left[(v/v_d)^\delta - 1)\right]^2 \tag{16}$$

The purpose of the weighting factors δ^2 and γ are to ensure that the model gives similar behaviour to the IDM for a given parameter set v_d, u_a, u_b, s_0, τ and δ. Derivation of these weighting functions and comparisons between this model, the IDM, and naturalistic driving data may be found in [16]. Finally, the third and fourth terms are quadratic penalties on the control inputs of acceleration and braking.

To complete the model of driver preferences, we add constraints on lateral acceleration while cornering, based on the model in [21]. This is equivalent to the following inequality constraint on the lateral acceleration u_y

$$u_y = |\kappa(x)| v^2 \leq \Gamma - \Delta v^2 \tag{17}$$

where $\kappa(x)$ is the road curvature, a function of the travelled distance, Γ is the driver's maximum comfortable lateral acceleration while cornering, and Δ is the driver's "safety margin" of error in their estimate of the curvature when approaching the corner. This may be restated as a speed constraint

$$v \leq \sqrt{\frac{\Gamma}{|\kappa(x)| + \Delta}} \tag{18}$$

which is suitable for inclusion in the optimal control problem. Speed is also constrained to comply with road regulations as:

$$v \leq v_{\max}(x) \tag{19}$$

Note that, without any loss of generality, we may assume that $v_{\max}(x)$ is defined such that it also incorporates the speed constraints resulting from the curvature, (18). Finally, we include a safety constraint on headway distance, which forces the model to perform emergency braking if required

$$s = x_l - x \geq s_0 \tag{20}$$

where x is the position of the front of the ego vehicle, while x_l is the position of the back of the leading vehicle.

B. Energy loss model

Minimisation of battery current or power usage is typically difficult when using direct solvers for optimal control, as the resulting optimisation is highly nonconvex in vehicle force and velocity. This typically leads to poor convergence and numerical problems in nonlinear programming solvers such as IPOPT, which is used later in the example. For use in an OCP, we approximate the energy losses in the powertrain due to the EV model of Section II, rather than minimising utilised battery current or energy. Although the resulting problem is still nonconvex in general, bilinear terms such as $P = Fv$ are typically less dominant giving more reliable convergence to a local minimum in practice. Considering conservation of energy, the total energy usage (10) may be rewritten as

$$E_b = \int_0^T (L_v + L_e + L_i)\, dt + \frac{1}{2} m (v_T^2 - v_0^2) + mg(h_T - h_0) \tag{21}$$

where L_v, L_e, L_i denote the vehicle power losses, powertrain losses, and idle losses respectively and the final two terms represent changes in kinetic and gravitational potential energy over the journey. If the initial and final vehicle speeds v_0 and v_T and elevations h_0 and h_T are known, then the final two terms are fixed. This means that minimising the integral of the losses $L = L_v + L_e + L_i$ is equivalent to minimising E_b within the stage cost of an OCP.

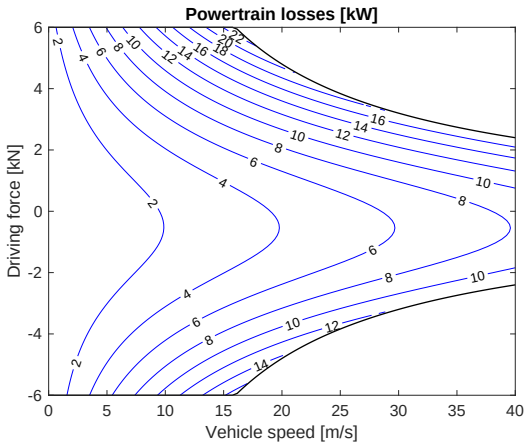

Fig. 5. Approximated powertrain losses as a function of vehicle speed and electrical traction force. Note the asymmetry, caused by the battery power and current values being larger in magnitude under traction than braking.

Vehicle losses L_v include those due to mechanical braking, rolling resistance, and aerodynamic drag:

$$L_v = \left(F_f + mgc_{rr} + \frac{1}{2}\rho C_d A v^2 \right) v \tag{22}$$

For optimal control, we approximate the true powertrain losses by a polynomial in $F_m = F_p - F_r$ and v. In our work, this polynomial was determined empirically by fitting a loss function L_e using all polynomial coefficients up to 3rd order in F_m and v, removing any coefficients with a p-value of greater than 0.05. The least-squares fit was then repeated with this reduced set of terms. This gave a function of the form

$$L_e = a_{01}v + a_{11}F_m v + a_{20}F_m^2 + a_{30}F_m^3 + a_{21}F_m^2 v \tag{23}$$

with coefficients as shown in Table II for the case in which F_m is measured in units of kN and v in m/s. This produced a good fit to the losses of our case study powertrain using the empirical ADVISOR data for the electric motor, with $R^2 = 0.971$, and gave an approximate powertrain loss function to be used in the optimal control problem, as shown in Figure 5. Although it was obtained empirically, we can

TABLE II
COEFFICIENTS OF POWERTRAIN LOSS MODEL

Coefficient	Value and 95% Confidence interval)
a_{01}	0.0207 (0.0152, 0.0261)
a_{11}	0.0308 (0.0260, 0.0356)
a_{20}	0.0207 (0.0152, 0.0261)
a_{30}	0.00167 (0.000912, 0.00243)
a_{21}	0.0279 (0.0268, 0.0291)

ascribe a physical basis to many terms in (23). For example, $a_{11} \approx 0.03$ is expected from the 97% combined efficiency of the mechanical transmission and power electronics $\eta_t \eta_{pc}$, while the presence of v, F^2 and $F^2 v$ terms are expected from static friction, Ohmic and hysteresis losses respectively in the electric motor. It is also possible to fit the data using convex functions. However, this produced a much poorer fit to the powertrain loss data with only $R^2 = 0.74$, so we elected to retain the nonconvex formulation in our test cases.

C. Inclusion of braking bias constraints

As the driver preference model is expressed as the minimisation of a loss function (13), it is straightforward to blend the two objectives of satisfying the driver's preferences and minimising energy losses in an OCP. This leads to a combined loss function to be minimised:

$$J = \int_0^T \left[(1-w)L_d + w\frac{L_v + L_e + L_i}{L_0} \right] dt \tag{24}$$

The weighting factor w is introduced to balance the two stage cost functions: $w = 0$ describes a naturalistic driving problem, $w = 1$ corresponds to an energy minimisation problem, while intermediate values $0 < w < 1$ represent a compromise between naturalistic driving and energy efficiency; constant L_0 is not necessary, but is helpful in practice to adjust for the differing units and scalings.

The motion of the vehicle is described in terms of the speed v and travelled space x, which are controlled by the force at the wheels $F = F_p - F_r - F_f$ according to

$$f_1: \quad \dot{x} = v \tag{25a}$$

$$f_2: \quad m\dot{v} = F - \frac{1}{2}\rho C_d A v^2 - c_{rr}mg - mg\theta \tag{25b}$$

where aerodynamic, rolling resistance and road gradient forces are accounted for according to (1), using a small angle approximation $\cos\theta \approx 1$, $\sin\theta \approx \theta$. As the vehicle is assumed to be front-wheel drive, the braking bias relationship (12) places an effective limit on the proportion of braking that may be regenerative, with some mechanical braking required at the rear wheels required to maintain directional stability. Within the OCP, we wish to satisfy the equality (12) except when this would exceed torque or power limits, so that

$$F_r = \min(\beta_r(F_r + F_f), F_{r,\max}) \tag{26}$$

where $F_{r,\max} = \min\left(T_{r,\max}N/r, P_{r,\max}/v\right)$, based on the torque and power limits $T_{r,\max}$ and $P_{r,\max}$ of the motor respectively. Unfortunately, including (26) as an equality constraint in the resulting OCP, or using this equality to eliminate one of the OCP inputs, typically leads to a problem that is difficult to solve numerically. Instead, we consider a relaxation of the OCP with an inequality constraint for the braking bias:

$$F_r \leq \beta_r(F_r + F_f) \tag{27}$$

Typically, unless motor torque or power constraints prohibit it, this constraint is satisfied with equality in the OCP solution, as regenerative braking is preferred over mechanical braking when minimising L_e. In that case, the equality (12) is recovered while retaining a problem formulation that is amenable to solution using direct methods.

D. Implementation and computational considerations

When using F_p, F_r, and F_f as control inputs, we consider a minor modification to the driver behaviour model in [16] and

redefine L_d according to

$$L'_d = \delta^2 \left(\frac{v}{v_d} - 1\right)^2 + \gamma(v)\ \frac{(s/s_d - 1)^2}{(s/s_d)^2 + 1} + \left(\frac{F_p}{mu_a}\right)^2 + \left(\frac{F_r}{mu_b}\right)^2 + \left(\frac{F_f}{mu_b}\right)^2 \quad (28)$$

with separate terms for the components of vehicle acceleration corresponding to the propulsive, regenerative braking and mechanical braking force inputs. This modification has a negligible effect on the resulting driving behaviour, while having separate quadratic penalties on each input improves numerical performance. The full OCP, which has two states (x, v) and three inputs (F_p, F_r, F_f), can be stated as

$$\min_{F_p,F_r,F_f} J = \int_0^T \left[(1-w)L'_d + w\frac{L_e + L_v + L_i}{L_0}\right] dt \quad (29a)$$

$$\text{s.t.} \quad \dot{x} = v$$
$$m\dot{v} = F_p - F_r - F_f - \frac{1}{2}\rho C_d A v^2 - mg\left[c_{rr} + \theta(x)\right] \quad (29b)$$

$$\begin{aligned} &x \le x_l(t) - s_0, \quad 0 \le v \le v_{\max}(x) \\ &0 \le rF_p \le N\,T_{m,\max}, \quad 0 \le F_f \\ &0 \le rF_r \le N\,T_{r,\max}, \quad (1-\beta_r)F_r \le \beta_r F_f \\ &-P_{r,\max} \le (F_p - F_r)v \le P_{m,\max} \end{aligned} \quad (29c)$$

Boundary conditions are added for each scenario, and will be specified in the following sections for our examples.

The problem is inherently nonconvex due to the nature of the powertrain and braking losses and constraints. As we retain this nonconvexity, there is no guarantee that a solution found by a direct method to solve the OCP is a global minimum. Nonetheless, we find that implementations of (29) perform well in practice. due to the formulation in terms of energy losses L, and the relaxation of the brake bias constraint. When performing collocation and mesh refinement using an hp-adaptive solver (GPOPS-II [22] in our examples) with the interior point NLP solver IPOPT used to solve the resulting optimisation problems, A single instance of (29) for a long-horizon scenario with 25 km of driving taking approx. 20 minutes of simulation time was solved in approximately 2 minutes on a standard desktop PC equipped with a 9th generation intel i5 processor, corresponding to solution approximately 10 times faster than real time. In contrast, equivalent formulations directly minimising P and/or using F_b as a control input rather than F_r and F_f were found to take an order of magnitude longer to solve, with IPOPT often failing by converging to an infeasible point in our numerical experiments.

Basic numerical efficiency improvements were implemented to speed up evaluation of the cost and constraint functions in our implementation. This included 'inlining' evaluation of the loss functions (22), (23) and (28) to avoid function call overheads. Another adjustment is made in the evaluation of (16), where the exponentiation $(v/v_d)^\delta$ is typically a slow step. Yet as typically $\delta = 4$ in the IDM, this may be replaced by two multiplications of the form $(v/v_d)^2 = (v/v_d)(v/v_d)$ and $(v/v_d)^4 = (v/v_d)^2(v/v_d)^2$, which is much faster to evaluate. As these functions and their derivatives are evaluated many times via callbacks during optimisation using IPOPT, these minor modifications lead to significant speed improvements.

IV. Test cases and driving scenario example

The OCP (29) is a multi-objective optimisation, that minimises both energy losses and deviations from a naturalistic driving model. In car-following scenarios, this driving model is meant to replicate the popular Intelligent Driver Model (IDM) for traffic modelling in car-following situations. Therefore, with the desired speed v_0 set high, it may be expected to maximise average speed subject to maintaining reasonable car-following distances and cornering speeds. Accordingly, in this section we investigate the Pareto-optimal frontier of energy usage $E_0 i_b$ versus average speed, in which the average speed is optimised indirectly via minimisation of L'_d. This multi-objective optimisation is considered in several examples, before investigating the results in a realistic, long-horizon scenario involving a 25 km drive through rural, highway and urban roads. Results for all cases are summarised in Table III.

TABLE III
Summary of results for all test cases

	Energy usage [kWh/km]	**Average speed [km/h]**	**Trip length [km]**
Cornering			
$w = 0$	0.153	62.1	0.8
$w = 0.5$	0.118	58.7	0.8
$w = 1$	0.068	42.0	0.8
Corner & follow			
$w = 0$	0.134	58.3	0.8
$w = 0.5$	0.116	58.3	0.8
$w = 1$	0.066	41.1	0.8
Car-following			
$w = 0$	0.145	62.6	4.4
$w = 0.5$	0.106	60.7	4.4
$w = 1$	0.095	54.8	4.4
Whole journey			
$w = 0$	0.181	78.5	25
$w = 0.5$	0.143	72.9	25
$w = 1$	0.123	65.1	25

A. Cornering case

In this scenario, the road consists of two straight segments joined in the middle by a 90° curve with a radius of approximately 30m. The total length of road is $l = 800$ m, the road elevation is constant $\theta(x) = 0$. We assume that there is no traffic, except for the ego-vehicle, and the boundary conditions of the OCP problem (29) are set to the following

$$\begin{aligned} x(0) &= 0 \quad & x(T) &= l \\ v(0) &= v_0 \quad & v(T) &= v_0 \end{aligned} \quad (30)$$

where T is the travel time, and v_0 is the initial and final speed (which are equal), all of which are free and will be determined in the optimisation. The initial and final speed are free but have been set to the same value. This can be interpreted as a search for optimal periodic solutions – as if driving on a road with many such curves, each separated by 800 m. We note also that as initial and final speeds are equal, there is no variation of the kinetic energy, which ensures that the energy losses may be

minimised in place of energy usage, according to (21). The speed is limited by the cornering constraint (18) defined in Section III, and it is also limited by the speed limit constraint (19), which is artificially set just above the legal speed limit in this case, to illustrate that the OCP solution will follow the drivers preferred speed v_d when the speed limit constraint $v_{\max}(x)$ is set higher than v_d. This means that the constraint $v \leq v_{\max}(x)$is inactive except in the corner.

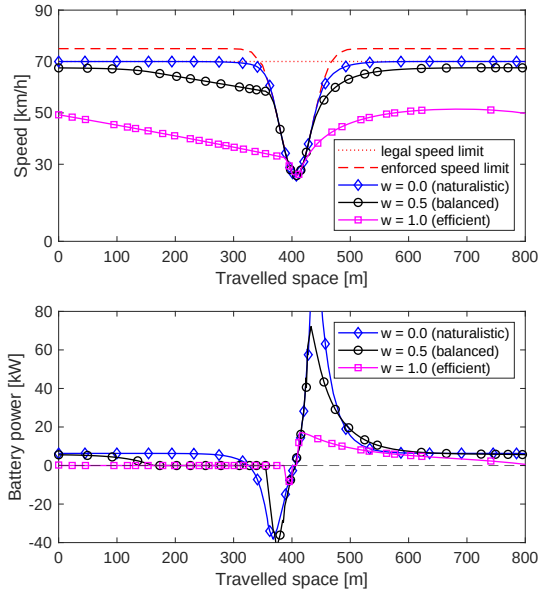

Fig. 6. Solution of the cornering case for three different combinations of driving preferences and energy economy.

Figure 6 shows the results of the optimisation in the limit cases of $w = 0$ (driver model only, i.e. "naturalistic" driving) and $w = 1$ (minimisation of energy loss only, "efficient" driving), plus an intermediate case with $w = 0.5$ (both driver preferences and energy efficiency considered, "balanced" driving). The optimised driving behaviour has been found by solving the OCP (29), with the battery power usage $E_0 i_b$ evaluated using the original current usage function (8) as detailed in Section II. Comparing the naturalistic and energy-efficient cases, efficient driving may save 56% energy at the cost of a 48% increase in the travel time. However a better compromise may be found between travel time and energy usage: the $w = 0.5$ case which blends the two objectives manages to save 23% electrical energy with only a 6% increase in travel time. This improvement is attributable to the introduction of coasting behaviour before the curve, thereby avoiding large energy losses due to braking.

As the driver model L'_d is being used in these optimisations as a 'surrogate' loss function for minimising the travel time, it is also interesting to compare the behaviour of OCP (29) with the alternative of minimising travel time directly in the OCP, i.e. replacing the OCP cost function with:

$$J' = (1-w)T + w\int_0^T \frac{L_e + L_v + L_i}{L_0}\, dt \qquad (31)$$

A comparison of the Pareto frontier for this 'minimum time' optimisation and OCP (29) is given in Figure 7. The Pareto curves are seen to be very similar, diverging only near $w = 0$. From inspection of the solutions, the difference between the two in the $w = 0$ case is attributable to two aspects: a) that the minimum time solution goes above the legal speed limit (noting that $v_d = 70$ km/h in the driver model prevents this), and b) the minimum time solution exceeds the driver's desired acceleration and braking accelerations u_a and u_b. In another test, the authors verified that increasing u_a, u_b and v_d in the driver model made the two curves overlap also near $w = 0$. We also note that in the minimum time case, the solution for $w = 0.001$ had to be used in place of $w = 0$ due to some ill conditioning when solving with the minimum-time cost only.

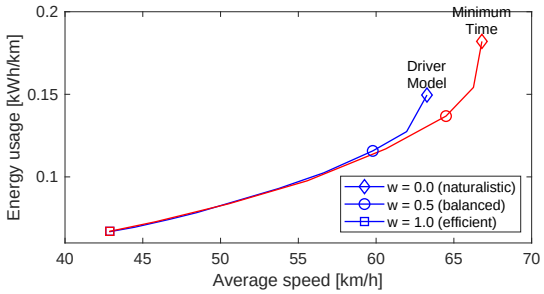

Fig. 7. Pareto comparison of driver model with minimum time optimisation.

B. Cornering with following case

We now consider a modification of the cornering scenario in which the ego vehicle is following another leader vehicle on the same section of road. The leader travels at an average speed of 60 km/h with the speed profile shown in Figure 8 by the blue dashed line, which has sections of deceleration, acceleration and constant speed. The initial travelled distance of the leader vehicle is set as $x_l(0) = 10$, so that the leader vehicle is initially 10 m in front of the ego vehicle. Other boundary conditions are identical to the previous case.

Results are shown in Figure 8, in which it is apparent that similar coasting and speed reduction behaviours are found to the non-following case. Viewing the plot of headway distance, the energy-efficient case travels slowly and loses its proximity to the lead vehicle, while the naturalistic and blended cases follow it more closely. Interestingly, there is a minor difference in speed between the naturalistic and blended cases for approximately the first 150 m, where the naturalistic case slows down early to maintain distance from the lead vehicle and continues at a constant speed to the corner, while the blended case maintains the initial speed then follows the leader at a slightly reduced distance before starting to coast down before the corner. The difference from the cornering-only scenario is apparent when inspecting the Pareto frontier (Figure 9). Here, the Pareto curve is similar in both cases until the average speed is equal to that of the lead vehicle, at which point, further decreases in w lead to a small increase in energy usage without any corresponding increase in average speed, due to this being constrained by the lead vehicle. Therefore the blended case compares favourably with the naturalistic one in this scenario, giving a 13% reduction in energy usage with no reduction in average speed.

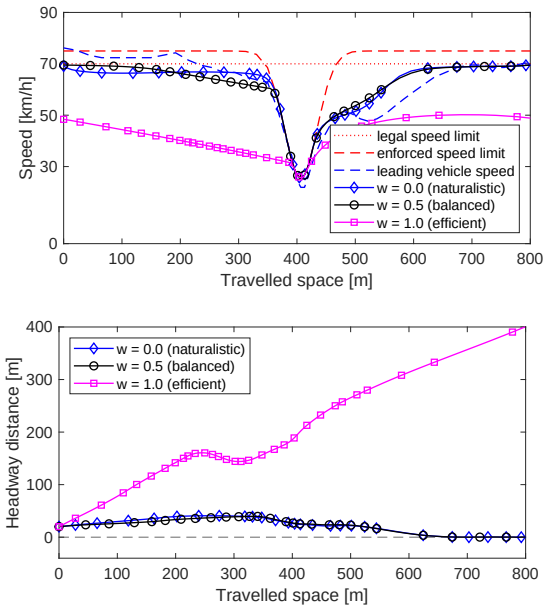

Fig. 8. Solution of the cornering with following case for three combinations of driving preferences and energy economy.

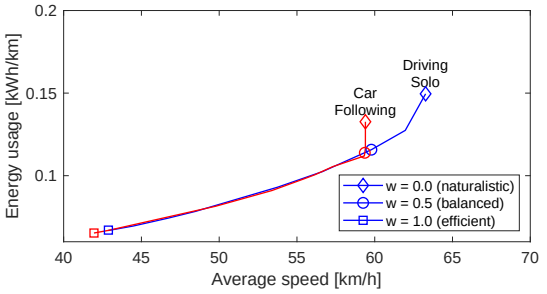

Fig. 9. Pareto comparison of cornering and cornering with following cases

C. Car-following case

We now consider a more complex, car-following scenario on $l = 4.5$ km of rural road, with a lead vehicle following a velocity profile obtained from real-world driving data. The ego vehicle is now assumed to be stationary at the start and end of the simulation, with the boundary conditions

$$\begin{aligned} x(0) &= 0 \quad x(T) = l \\ v(0) &= 0 \quad v(T) = 0 \end{aligned} \tag{32}$$

where T denotes the travelling time that, once again, is taken as a free variable. Cornering constraints are imposed, which correspond to the measured curvature of corners on the same rural route that the lead vehicle followed during data collection. Results are shown in Figure 10, which shows the speed and headway distance to the lead vehicle in the naturalistic, energy-efficient and blended cases. In the energy efficient case, it is apparent that the ego vehicle is no longer following the lead vehicle, as the headway distance increases considerably. As in the previous cornering scenarios, it is clear that the blended case achieves significant reductions in energy usage of 24% with only a 3% increase in travel time. Inspecting the Pareto frontier of the multiobjective problem in Figure 11, we observe that for low values of w, e.g. $w = 0.1$ and $w = 0.2$, there is a considerable improvement in energy usage with almost no corresponding increase in travel time.

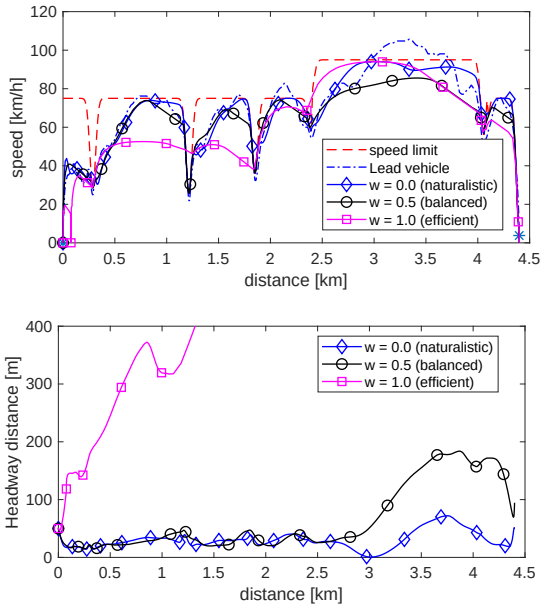

Fig. 10. Solution of the car-following case for three combinations of driving preferences and energy economy.

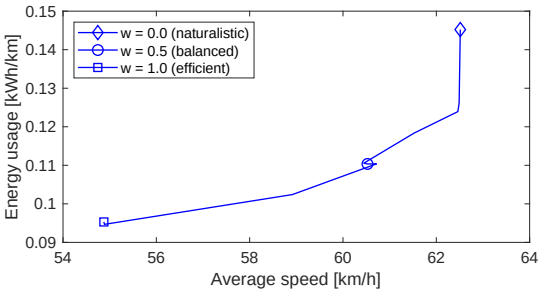

Fig. 11. Pareto frontier in the car-following case, 4.5 km of rural road

D. Eco-driving optimisation of a whole journey

To illustrate the scalability of OCP (29) in practice and give an indication of the potential energy savings possible in electric vehicles over a typical journey, we now consider a long horizon optimisation example, representing a full journey made near Padova (IT) along a route consisting of a 7 km rural section, a 14 km motorway section, and a 4 km urban section, for a total of approximately $l = 25$ km of driving. Boundary conditions are the same as in the car-following case (32), where travel time T was considered as a free variable, while the initial and final speeds were fixed at zero, which once again allows the energy losses to be minimised in place of the energy usage in the OCP.

It is unrealistic to assume that the ego-vehicle will follow the same lead vehicle for an entire long journey. Nonetheless, it is important to take traffic conditions into account in the eco-driving problem to ensure a realistic solution. While the incorporation of predicted traffic conditions into the eco-driving

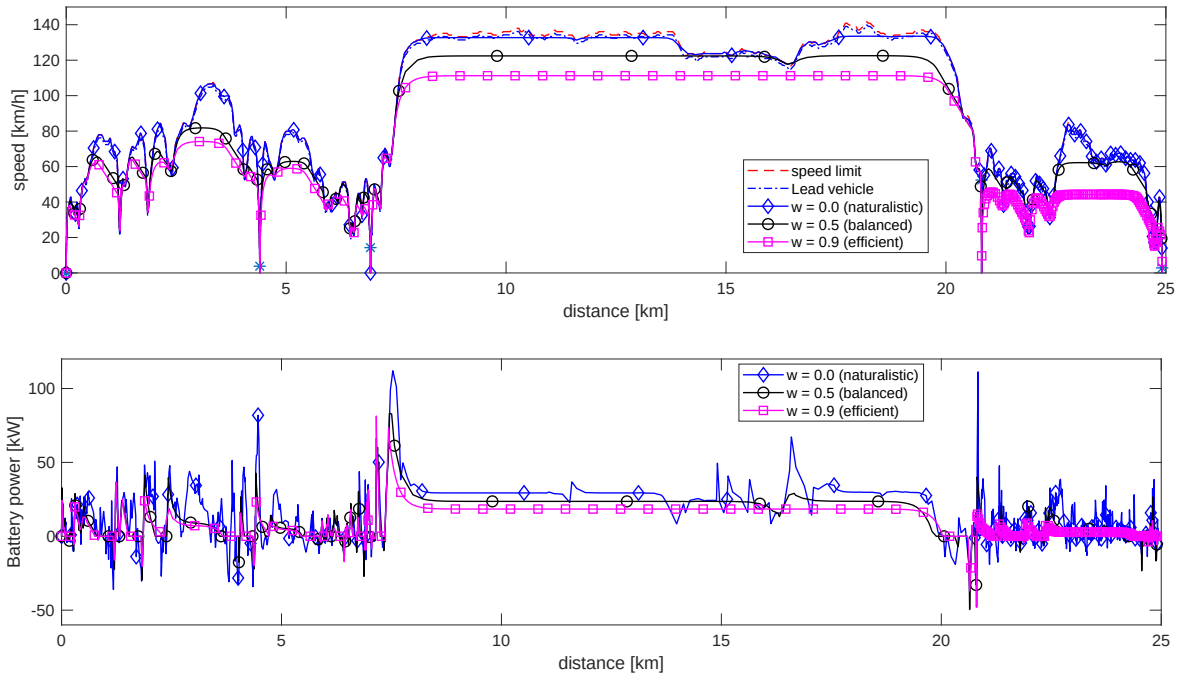

Fig. 12. Solution of the whole journey problem. Stars $*$ denote the 'stop signs' at the approximate start and end of each subsection of the journey.

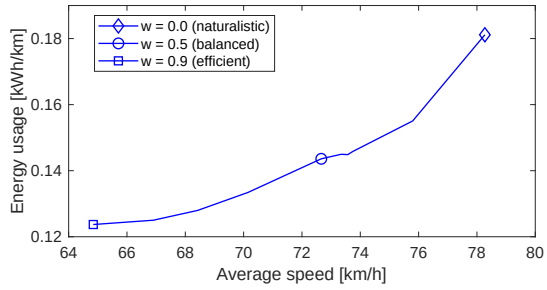

Fig. 13. Pareto comparison, 25 km driving scenario

problem in general is a open problem, for this example we account for them by introducing an additional maximum speed constraint that constrains the vehicle to travel slower than the average speed of traffic in each location, i.e. $v \leq v_{\text{traffic}}(x)$, with the traffic velocity obtained from real-world driving data along the route. The route contained several necessary stops at traffic signals and/or stop signs, and the ego-vehicle must make stops at these locations. This allows the problem to be broken down into several sub-problems for efficient solution, in which the optimisation is solved between stops, with the same boundary conditions, and the full solution constructed by stitching together the solutions to the sub-problems. In this example, these sub-problems corresponded to rural, motorway and urban sections of the route, with the rural section split into two parts due to a stop sign.

The optimal control problem was solved for values of $w = 0.0, 0.1, \ldots, 0.9$, with the resulting energy usage again evaluated according to the electric vehicle model described in Section II. A subset of the results illustrating naturalistic, energy-efficient and blended cases is shown in Figure 12. As in the previous examples, coasting behaviour is evident in the blended and energy-efficient cases. The Pareto optimal frontier is shown in Figure 13. For the blended case of $w = 0.5$, there is a 21% energy saving compared to the naturalistic driving case, with only a 7.1% decrease in average speed, corresponding to approximately 90 seconds of additional journey time on a journey of 19 minutes and 6 seconds (for the $w = 0$ case).

V. Conclusions

An eco-speed advisory system for front-wheel drive electric vehicle was developed that accounts for desired following distances and time headways, a desired vehicle speed, smooth vehicle acceleration, and a comfortable corner negotiation speed. This was found to successfully blend driver preferences with energy-efficiency, achieving energy savings of 21% with only a 7% decrease in average speed over a 25km journey involving rural, motorway and urban sections, with improvements also in specific car-following and cornering scenarios.

Future work will focus on developing receding-horizon schemes to approximate the full-horizon solution, which would allow for the proposed OCP to be used as the basis for an eco-ACC or self-driving vehicle subsystem. Computational results in the present paper were promising with effective solutions found on desktop PC hardware approximately 10 times faster than real time, implying that specialised online solvers, for example using nonlinear MPC, could achieve similar results in practical implementations.

Acknowledgment

This work was partially supported by the Engineering and Physical Sciences Research Council (EPRSC) EP/N022262/1.

REFERENCES

[1] F. Chen, N. Taylor, and N. Kringos, "Electrification of roads: Opportunities and challenges," *Applied Energy*, vol. 150, pp. 109–119, 2015.

[2] A. E. Af Wåhlberg, "Long-term effects of training in economical driving: Fuel consumption, accidents, driver acceleration behavior and technical feedback," *Int. Journal of Industrial Ergonomics*, vol. 37, no. 4, pp. 333–343, 2007.

[3] W. Ke, S. Zhang, X. He, Y. Wu, and J. Hao, "Well-to-wheels energy consumption and emissions of electric vehicles: Mid-term implications from real-world features and air pollution control progress," *Applied energy*, vol. 188, pp. 367–377, 2017.

[4] A. Castaings, W. Lhomme, R. Trigui, and A. Bouscayrol, "Comparison of energy management strategies of a battery/supercapacitors system for electric vehicle under real-time constraints," *Applied Energy*, vol. 163, pp. 190–200, 2016.

[5] W. Shabbir and S. A. Evangelou, "Threshold-changing control strategy for series hybrid electric vehicles," *Applied energy*, vol. 235, pp. 761–775, 2019.

[6] Z. Wei, J. Xu, and D. Halim, "Hev power management control strategy for urban driving," *Applied energy*, vol. 194, pp. 705–714, 2017.

[7] Y.-H. Hung and C.-H. Wu, "An integrated optimization approach for a hybrid energy system in electric vehicles," *Applied energy*, vol. 98, pp. 479–490, 2012.

[8] L. Zhao and J. Sun, "Simulation framework for vehicle platooning and car-following behaviors under connected-vehicle environment," *Procedia-Social and Behavioral Sciences*, vol. 96, pp. 914–924, 2013.

[9] J. Han, Y. Park, and Y.-s. Park, "Adaptive regenerative braking control in severe cornering for guaranteeing the vehicle stability of fuel cell hybrid electric vehicle," in *2011 IEEE Vehicle Power and Propulsion Conference*. IEEE, 2011, pp. 1–5.

[10] C. Sun, S. J. Moura, X. Hu, J. K. Hedrick, and F. Sun, "Dynamic traffic feedback data enabled energy management in plug-in hybrid electric vehicles," *IEEE Transactions on Control Systems Technology*, vol. 23, no. 3, pp. 1075–1086, 2015.

[11] M. A. S. Kamal, M. Mukai, J. Murata, and T. Kawabe, "Ecological vehicle control on roads with up-down slopes," *IEEE Transactions on Intelligent Transportation Systems*, vol. 12, no. 3, pp. 783–794, 2011.

[12] L. L. Ojeda, J. Han, A. Sciarretta, G. De Nunzio, and L. Thibault, "A real-time eco-driving strategy for automated electric vehicles," in *Decision and Control (CDC), 2017 IEEE 56th Annual Conference on*. IEEE, 2017, pp. 2768–2774.

[13] J. Han, A. Sciarretta, L. L. Ojeda, G. De Nunzio, and L. Thibault, "Safe- and eco-driving control for connected and automated electric vehicles using analytical state-constrained optimal solution," *IEEE Transactions on Intelligent Vehicles*, vol. 3, no. 2, pp. 163–172, 2018.

[14] M. A. S. Kamal, M. Mukai, J. Murata, and T. Kawabe, "Model predictive control of vehicles on urban roads for improved fuel economy," *IEEE Trans. on control systems technology*, vol. 21, no. 3, pp. 831–841, 2013.

[15] J. M. Fleming, C. K. Allison, X. Yan, N. A. Stanton, and R. Lot, "Adaptive driver modelling in ADAS to improve user acceptance: A study using naturalistic data," *Safety Science*, 2018.

[16] J. Fleming, X. Yan, and R. Lot, "Incorporating driver preferences into eco-driving assistance systems using optimal control," *IEEE Trans. on Intelligent Transportation Systems*, vol. 22, no. 5, pp. 2913–2922, 2020.

[17] K. B. Wipke and M. R. Cuddy, "Using an advanced vehicle simulator (advisor) to guide hybrid vehicle propulsion system development," National Renewable Energy Lab., Golden, US, Tech. Rep., 1996.

[18] M. Ehsani, Y. Gao, S. Longo, and K. Ebrahimi, *Modern electric, hybrid electric, and fuel cell vehicles*. CRC Press, 2018.

[19] G. Rill, *Road vehicle dynamics*. CRC Press, 2011.

[20] M. Treiber, A. Hennecke, and D. Helbing, "Congested traffic states in empirical observations and microscopic simulations," *Physical review E*, vol. 62, no. 2, p. 1805, 2000.

[21] G. Reymond, A. Kemeny, J. Droulez, and A. Berthoz, "Role of lateral acceleration in curve driving: Driver model and experiments on a real vehicle and a driving simulator," *Human factors*, vol. 43, no. 3, pp. 483–495, 2001.

[22] M. A. Patterson and A. V. Rao, "GPOPS-II: A MATLAB software for solving multiple-phase optimal control problems using hp-adaptive gaussian quadrature collocation methods and sparse nonlinear programming," *ACM Trans. on Mathematical Software*, vol. 41, no. 1, p. 1, 2014.

Roberto Lot received a Master's Degree cum laude in Mechanical Engineering in 1994 and a PhD in Mechanics of Machines in 1998 from the University of Padova, Italy.

From 2014 to 2019 he was Professor of Automotive Engineering at the University of Southampton, UK. Currently he is within the Department of Industrial Engineering at the University of Padova. His research interests include dynamics and control of road and race vehicles and contributions to make our vehicles safer, faster, and more eco-friendly. He has directed several national and international research projects and published more than 100 scientific papers.

James Fleming received the M.Eng. and D.Phil. degrees in Engineering Science from the University of Oxford, UK, in 2012 and 2016, respectively, before working as a Research Fellow at the University of Southampton, UK until September 2019.

Since then, he has been a Lecturer with the Wolfson School of Electrical, Mechanical, and Manufacturing Engineering, Loughborough University, UK. His research interests include developing theory and algorithms for optimal control, model predictive control, and reinforcement learning, with applications in the automotive and renewable energy sectors. He is author of over 30 peer-reviewed publications including 15 published in IEEE conferences and journals, and currently leads the "Learning of safety critical model predictive controllers for autonomous systems" project funded by the UK Engineering and Physical Sciences Research Council.

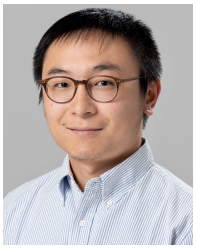

Boli Chen (M'16) received the B. Eng. in Electrical and Electronic Engineering in 2010 from Northumbria University, UK. In 2011 and 2015, he respectively received the MSc and the Ph.D. in Control Systems from Imperial College London, UK. Currently, he is a Lecturer in the Department of Electronic and Electrical Engineering, University College London, U.K. He is also an associate editor of the European Journal of Control and an associate editor of the EUCA Conference Editorial Board. His current research focuses on control, optimisation and estimation of complex dynamical systems, mainly from intelligent mobility and smart grid areas.

Simos A. Evangelou (Senior Member, IEEE) received the B.A. and M.Eng. degrees in electrical and information sciences from the University of Cambridge, Cambridge, U.K., in 1999, and the Ph.D. degree in control engineering from Imperial College London, London, U.K., in 2004. He is currently a Reader with the Department of Electrical and Electronic Engineering, Imperial College London. He is a member of the IFAC Technical Committee Automotive Control and on the Editorial Board of international journals and conferences, including the IEEE TRANSACTIONS ON CONTROL SYSTEMS TECHNOLOGY and the IEEE Control Systems Society Conference Editorial Board.